AIP Advances

A comparative study of transport properties of monolayer graphene and AlGaN-GaN heterostructure

Cite as: AIP Advances **5**, 077101 (2015); https://doi.org/10.1063/1.4926341
Submitted: 05 May 2015 . Accepted: 23 June 2015 . Published Online: 01 July 2015

M. D. Ozdemir, O. Atasever, B. Ozdemir, Z. Yarar, and M. Ozdemir

COLLECTIONS

Paper published as part of the special topic on Chemical Physics, Energy, Fluids and Plasmas, Materials Science and Mathematical Physics

View Online Export Citation CrossMark

ARTICLES YOU MAY BE INTERESTED IN

Mobility and saturation velocity in graphene on SiO_2
Applied Physics Letters **97**, 082112 (2010); https://doi.org/10.1063/1.3483130

Effective mass of electron in monolayer graphene: Electron-phonon interaction
Journal of Applied Physics **113**, 043708 (2013); https://doi.org/10.1063/1.4789385

Comparison of mobility extraction methods based on field-effect measurements for graphene
AIP Advances **5**, 057136 (2015); https://doi.org/10.1063/1.4921400



AIP Publishing

© 2015 Author(s).

A comparative study of transport properties of monolayer graphene and AlGaN-GaN heterostructure

M. D. Ozdemir,[1] O. Atasever,[2] B. Ozdemir,[2] Z. Yarar,[3] and M. Ozdemir[2,a]
[1]*Department of Physics, Faculty of Arts and Sciences, Aksaray University, 68100 Aksaray, Turkey*
[2]*Department of Physics, Cukurova University, 01330 Adana, Turkey*
[3]*Department of Physics, Faculty of Arts and Sciences, Mersin University, Çiftlikköy 33343 Mersin, Turkey*

(Received 5 May 2015; accepted 23 June 2015; published online 1 July 2015)

The electronic transport properties of monolayer graphene are presented with an Ensemble Monte Carlo method where a rejection technique is used to account for the occupancy of the final states after scattering. Acoustic and optic phonon scatterings are considered for intrinsic graphene and in addition, ionized impurity and surface roughness scatterings are considered for the case of dirty graphene. The effect of screening is considered in the ionized impurity scattering of electrons. The time dependence of drift velocity of carriers is obtained where overshoot and undershoot effects are observed for certain values of applied field and material parameters for intrinsic graphene. The field dependence of drift velocity of carriers showed negative differential resistance and disappeared as acoustic scattering becomes dominant for intrinsic graphene. The variation of electron mobility with temperature is calculated for intrinsic (suspended) and dirty monolayer graphene sheets separately and they are compared. These are also compared with the mobility of two dimensional electrons at an AlGaN/GaN heterostructure. It is observed that interface roughness may become very effective in limiting the mobility of electrons in graphene. © *2015 Author(s). All article content, except where otherwise noted, is licensed under a Creative Commons Attribution 3.0 Unported License.* [http://dx.doi.org/10.1063/1.4926341]

I. INTRODUCTION

Graphene, a truely two dimensional material with a linear energy dispersion without any gap is synthesized for the first time by Novoselov et al.[1] Since its invention many interesting properties of graphene are reported both from the stand points of theory and experiment.[1–4] It is flexible yet much stronger than steel,[5] it is a good conductor of both heat and electricity and it conducts electricity better than copper.[6] While its room temperature mobility is reported for the case of dirty graphene to be around 10^4 cm^2/V·s,[7–10] mobility values up to 10^5 cm^2/V·s are reported for clean suspended graphene samples at low carrier densities of $\sim 10^{12}$ cm^{-2}.[6,11–14]

Charge transport and mobility characteristics of graphene are studied by Monte Carlo (MC) techniques by a number of researchers.[15–18] The carrier transport problem is investigated for an intrinsic graphene sample by an ensemble MC technique in Ref. 15 where acoustic and optic phonon scatterings are taken into account. They found that velocity saturation in graphene occurs at relatively low electric fields but the value of the field is dependent on the carrier density. The high field transport of carriers in intrinsic graphene is studied in Ref. 16 where in addition to acoustic and optic phonon scatterings, electron-electron scatterings are also taken into account. They found, among others, that phonon scattering is the dominant cause of velocity saturation in graphene and electron-electron scattering eliminates negative differential resistance (NDR) phenomenon in graphene. Another high field transport study is carried in Ref. 17 where in addition to acoustic and

[a]M. Özdemir, e-mail: metoz@cu.edu.tr

 ©Author(s) 2015

optic phonon scatterings the ionized impurity scattering is also considered. They found that the saturation current in graphene scales with the square root of the density of carriers. The effect of surface polar phonons on the transport and deformation potential constant measurements on various substrates is studied in detail in Ref. 18.

In the present study we investigate the charge transport and mobility charactheristics of monolayer graphene as a function of temperature and various material parameters using an ensemble MC method. We consider both the so called dirty graphene with impurities and an intrinsic graphene. We also make a distinction between a suspended graphene and graphene on a substrate. In the investigation of transport charactheristics of graphene the following scattering mechanism for electrons are taken into account: acoustic and optical phonon, charged impurity and interface roughness scatterings. The calculations were made with a suitable combination of analytical and numerical methods. In the case of ionized impurity scattering of electrons, the effect of screening is also considered. A rejection technique is used in MC simulations to account for the occupancy of the final states after scattering. The drift velocity of carriers are calculated as a function of time at a given value of applied field and from these, the steady state drift velocity-electric field curves are obtained for different temperatures. In addition, conductivity calculations are carried out in the presence of scattering mechanisms just mentioned for various material parameters and from these the mobility of carriers are determined. These mobility values are compared with that of a two dimensional electron gas confined at an AlGaN/GaN heterostructure.

The organization of the paper is as follows: In Section II we give briefly the scattering mechanisms, conductivity expressions and MC simulation method used in the study. Section III is devoted to results and dicussions where we present in detail the velocity-time and velocity-field characteristics of monolayer graphene in addition to mobility calculations where the mobility of intrinsic and dirty graphene is compared with the mobility of two dimensional carriers in an AlGaN/GaN heterostructure. Our conclusions are provided in Section IV.

II. THEORY

A. Scattering Mechanisms

The scattering mechanisms that are taken into account in the transport problem of electrons in monolayer graphene are as follows: scattering with lattice vibrations, Coulomb scattering with impurity charges and charge carrier interaction with rough interface. Among the the phonon interaction processes, we first consider the acoustic phonon scattering mechanism treated in the frame work of acoustic deformation potential approximation.[16,19] Acoustic scattering is considered to be elastic where the scattering rate linearly depends both on temperature and electron energy. At sufficiently high temperatures electron-acoustic phonon interaction can be significant especially in intrinsic graphene and therefore can be a major source of mobility limiting process. A linear dispersion relation for acoustic phonon frequency is assumed ($\omega_q = \upsilon_s q$) where υ_s is the sound velocity in graphene and q is the wavevector associated with the acoustic phonons. Longitudinal acoustic phonon scattering is given by[16,19]

$$W(k) = \frac{\pi D_{ac}^2 k_B T}{4\sigma \upsilon_s^2 \hbar^3 \upsilon_F^2} E_k \tag{1}$$

where both emission and absorption processes are considered. Here the energy of electrons is given as $E_k = \hbar \upsilon_F |\mathbf{k}|$ where υ_F is the Fermi velocity whose approximate magnitude is $\sim 10^6$ m/s, D_{ac} is the acoustic deformation potential constant, σ is the surface mass density of graphene sheet, k_B is the Boltzmann constant and T is the absolute temperature. The material parameters used in this study are provided in Table I.

The second phonon scattering mechanism we consider is the non-polar optical phonon scattering.[15,16] Non-polar optical phonons are treated inelastically in the simulations. Similar to the acoustic phonons, only longitudinal optic (LO) phonons contribute to the scattering of charge carriers. In this case the scattering rate is given by

TABLE I. Material parameters used in the study.

Electron concentration (n)	1×10^{12} cm^{-2}
Impurity concentration (n_i)	1.5×10^{11} cm^{-2}
Fermi velocity (v_F)	1×10^{6} m/s
Sound velocity (v_p)	1×10^{4} m/s
Optic phonon energy	152 meV
Optic deformation constant (D_o)	1×10^{9} eV/cm
Acoustic deformation constant (D_{ac})	3.7, 20 eV
Relative dielectric constant for graphene	$0.8\varepsilon_0$
Root mean square deviation of interface roughness (Δ)	5 Å
Lateral extent of roughness scattering (L_e)	1 nm
Gate induced carrier density (n_s)	1×10^{12} cm^{-2}

$$W(k) = \frac{D_0^2}{4\sigma\omega_0(\hbar\upsilon_F)^2}\{n_0(E_k+\hbar\omega_0)+(n_0+1)(E_k-\hbar\omega_0)\Theta(E_k-\hbar\omega_0)\} \tag{2}$$

where n_0 is the Bose-Einstein distribution function, D_0 is deformation potential constant for optic phonons and the Heaviside step function Θ ensures that phonon emission can occur only when the electron has sufficiently high energy ($E_k > \hbar\omega_0$).

The scattering mechanism we consider next is the scattering of charge carriers by the impurities. The impurities can be either in the monolayer graphene sheet and/or in the substrate that the graphene sheet resides on for the case of unsuspended graphene. The importance of impurity scattering and the effect of carrier density on impurity scattering was studied by different groups.[20–25] Charge impurities present in the substrate is one of the significant sources of mobility degradation in graphene. In the presence of screening the Fourier transform $V(\mathbf{q})$ of Coulomb scattering potential is given by

$$V(\mathbf{q}) = \frac{2\pi e^2}{\kappa q\epsilon(\mathbf{q})}\cdot\exp(-qd) \tag{3}$$

where d is the distance of charged impurities from the graphene sheet. The wave-vector $q = |\mathbf{k}'-\mathbf{k}| = 2k\sin\theta/2$, κ is the effective dielectric constant of the system (graphene and substrate) and $\epsilon(\mathbf{q})$ is the static dielectric function. θ is the angle between the electron wave vectors before ($\mathbf{k}$) and after ($\mathbf{k}'$) scattering. Starting from the Linhard function and under random phase approximation, $\epsilon(\mathbf{q})$ is given in terms of polarization function $\Pi(q)$ as:[4,26]

$$\epsilon(q) = 1+\frac{2\pi e^2}{\kappa q}\Pi(q) \tag{4}$$

$$\Pi(q) = \frac{g_v g_s}{2\pi\hbar\upsilon_F}\left\{\int_0^\infty f^+(\varepsilon_k) - \int_0^{q/2} f^+(\varepsilon_k)\sqrt{1-\left(\frac{2k}{q}\right)^2}\right\}dk \tag{5}$$

where $f^+(\varepsilon_k) = f(\varepsilon_k)+f(\varepsilon_k+2\mu)$ with $f(\varepsilon_k)$ being the Fermi-Dirac function. The scattering rate for (remote) impurity scattering in the presence of n_i impurity charge centers per area is given as:

$$W(k) = \frac{(n_i)E_k}{\pi\hbar^3\upsilon_F^2 k}\int_0^{2k}|V(\mathbf{q})|^2\left[1-\left(\frac{q}{2k}\right)^2\right]^{1/2}dq. \tag{6}$$

The last scattering mechanism we will consider is the interface roughness scattering. Interface roughness in graphene can occur due to intrinsic rippling effect and/or due to topography of the underlying substrate. For an exponential autocorrelation function ($\Delta(r) = \Delta_e^2 e^{-\sqrt{2}r/L_e}$) the power spectrum density $|\Delta(q)|^2$ is given by[27]

$$|\Delta(q)|^2 = \pi\Delta_e^2 L_e^2\left(1+\frac{L_e^2 q^2}{2}\right)^{-3/2} \tag{7}$$

where Δ_e is the root mean square (rms) height of interface, L_e is the correlation length of rough surface and n_s is induced carrier density. Under this function the interface roughness scattering rate

is calculated as:[27,28]

$$W(k) = \frac{E_k}{2\hbar}\left(\frac{\Delta_e L_e n_s e^2}{2\varepsilon\hbar\upsilon_F}\right)^2 \int_0^{\pi}\left(1 + 2L_e^2k^2\sin^2\frac{\theta}{2}\right)^{-3/2} \cdot (1+\cos\theta)\, d\theta. \tag{8}$$

The conductivity of graphene sheet can be calculated using the semi-classical diffusive equation[19]

$$\sigma = \frac{g_v g_s e^2}{h}\frac{E_F}{2\hbar}\langle\tau\rangle = \left(\frac{2e^2}{h}\right)\frac{E_F}{\hbar}\langle\tau\rangle \tag{9}$$

where $\langle\tau\rangle$ is the average scattering time given by[19]

$$\langle\tau\rangle = \frac{\int_0^{\infty} d\varepsilon\varepsilon\tau(\varepsilon)\left(-\frac{df}{d\varepsilon}\right)}{\int_0^{\infty} d\varepsilon\varepsilon\left(-\frac{df}{d\varepsilon}\right)} \tag{10}$$

where $f(\varepsilon)$ is the Fermi-Dirac function. The scattering times are calculated using the scattering rates given above as follows:

$$\frac{1}{\tau(\varepsilon)} = \sum_{i=1}\frac{1}{\tau_i} \tag{11}$$

where the sum is over all scattering mechanisms considered. The transport scattering times are calculated by multiplying the integrand in the derivation of equations (1), (2), (6), and (8) by the factor $(1-\cos\theta)$.

B. Ensemble Monte Carlo

An ensemble Monte Carlo technique is used to study the transport of electrons in monolayer graphene where the linear dispersion relation and the scattering mechanisms mentioned above are considered. A rejection technique is used in MC simulations to account for the occupancy of the final states after scattering. The drift velocity of carriers are calculated as a function of time at a given value of applied field to graphene sheet and from these, the steady state drift velocity-electric field curves are obtained for various temperature and material parameters. The number of particles used in the simulation is about 10^4. The drift velocity of electrons can be calculated using semi-classical equations of motion where the mass of particles is required. The motion of particles in graphene, however, is governed by Dirac equation where the particles mimic relativistic particles with zero rest mass. While the linear energy dispersion relation of electrons in graphene implies zero rest mass, their cyclotron mass is not zero and is given by $m^* = E/\upsilon_F^2$.[1] Therefore the drift velocity of electrons in graphene can be expressed as

$$\upsilon_d = \upsilon_F\frac{k_x}{|\mathbf{k}|} \tag{12}$$

where k_x is the wave vector in the direction of applied electric field.

The conductivity of electrons is calculated from equation (9) from which the mobility of electrons can be obtained using the relation

$$\mu = \frac{\sigma}{en} \tag{13}$$

where n is the density of electrons and e is the charge of an electron. The mobility of intrinsic graphene and graphene with impurities are studied as a function of temperature for various material parameters. The mobility values are compared with the mobility of two dimensional electrons in an AlGaN/GaN heterojunction.

III. RESULTS AND DISCUSSIONS

We first consider the velocity behaviour of an intrinsic graphene as a function of time where only acoustic and optic phonon scatterings are considered. The effect of substrate material is also

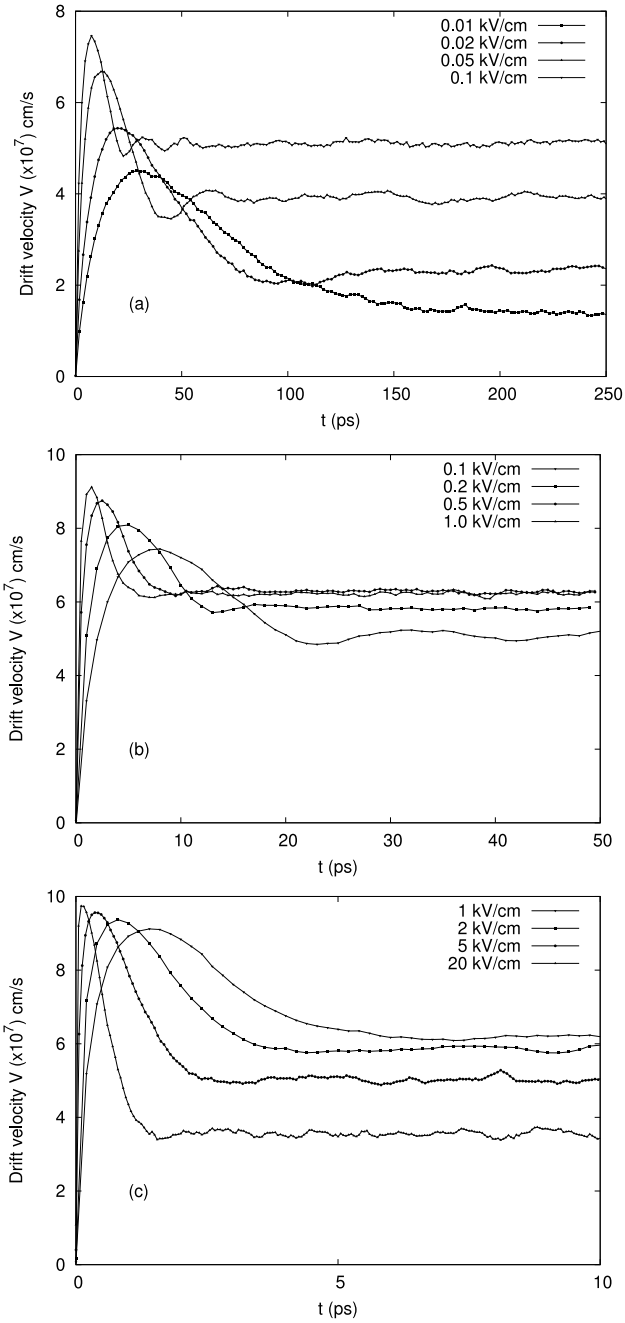

FIG. 1. Steady state velocity of graphene electrons as a function of time at various applied field values at room temperature (300 K). The number on the right hand corner indicates the applied field to graphene sample. Acoustic and optic deformation constants are $D_{ac} = 3.7$ eV and $D_o = 1 \times 10^9$eV/cm, respectively. Undershoot effect is visible between 0.02-1 kV/cm. Overshoot is observed at all field values, the peak velocity increases as the applied field increases, but the steady state velocity shows a negative differential resistance behaviour.

neglected so this corresponds to a so called suspended graphene. The results are depicted in three separate figures (Figures 1(a), 1(b) and 1(c)) to show more clearly the change in the behaviour of velocity charactheristics of graphene sheet as the applied field is increased. All results shown here are at T = 300 K where the acoustic deformation potential constant is D_{ac} = 3.7 eV and the optic deformation constant is taken to be $D_o = 1 \times 10^9$ eV/cm. An overshoot effect is observed for all fields considered. At low field values after a certain applied field ($\geq$ 20 V/cm) a so called

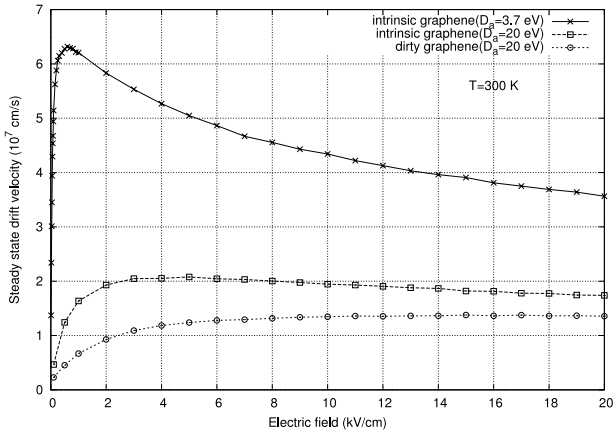

FIG. 2. The comparision of steady state drift velocities for intrinsic and dirty graphene with different material parameters. The curve with crosses where a negative differential resistance is observed corresponds to intrinsic graphene where only optic and acoustic phonon scattering are considered with the corresponding deformation potential constants of $D_{ac} = 3.7$ eV $D_o = 1 \times 10^9$ eV/cm, respectively. The curve with empty squares is for the case when $D_{ac} = 20$ eV for intrinsic graphene. Note that the NDR effect almost disappeared in this case. The curve with empty circles corresponds to dirty graphene where ionized impurity and interface roughness scatterings are also taken into account.

undershoot effect[29] sets in as can be seen in Fig. 1(a). This phenomenon persists until the applied field exceeds about 1 kV/cm. Further, as the applied field increases both the peak velocity and the steady state velocity increases up to the applied field of about 1 kV/cm (Figs. 1(a) and 1(b)), after which the peak velocity continues to increase but the steady state velocity decreases steadily as shown in Fig. 1(c). The steady state velocity-applied field curves corresponding to the situation shown in Fig. 1 can be seen in Fig. 2 (the curve with crosses) where an NDR behaviour can clearly be seen.

The acoustic scattering rate depends on the electron energy linearly. The optic scattering corresponding to emission process is the most effective scattering mechanism among the acoustic and optic scatterings. The optic phonon energy for emission process is about 0.15 eV, therefore the optic phonon scattering is not effective until the energy of a considerable amount of electrons used in the simulation gain enough energy compared to optic phonon energy. This happens at an applied field of 1 kV/cm or above. As one can see in Figures 1 and 2, at an applied field of about 1 kV/cm, the steady state velocity of carriers begin to decrease and hence NDR appears. The maximum steady state velocity attained is about 6.3×10^7 cm/s. The maximum overshoot velocity however is about 9.8×10^7 cm/s.

There is a range of values provided for acoustic deformation potential in the literature.[6,9] To see the effect of acoustic deformation potential on the steady state velocity of carriers as a function of applied field for the case of intrinsic graphene, we increased acoustic deformation potential value to D_{ac} = 20 eV keeping all other parameters as given in Fig. 1. When D_{ac} is increased the NDR phenomenon becomes very mild, the velocity of carriers decreases considerably and the field at which the peak velocity is attained shifts to higher field values (~ 5 kV/cm) (see the curve with empty squares in Fig. 2). Acoustic phonon scattering scales with the square of D_{ac}. When it is increased, acoustic phonon scattering becomes the dominant mechanism of scattering compared to optic phonons and therefore the NDR effect almost disappears.

We next consider the case of dirty graphene where the ionized impurity and interface roughness scatterings are considered. The screening effect is considered in ionized impurity scattering through equations (3), (4), and (5). The impurity concentration is taken to be 1.5×10^{11} cm^{-2} and the root mean square deviation of interface roughness and the lateral extent of roughness scattering are taken to be 5 Å and 1 nm, respectively. The steady state velocity as a function of applied field at T = 300 K is shown in Fig. 2 when D_{ac} = 20 eV (the curve with empty circles). For this case there is no observable NDR and the velocity is even lower compared to intrinsic graphene. For the present case the acoustic phonon scattering is too high so that the effect of optic phonons is suppressed.

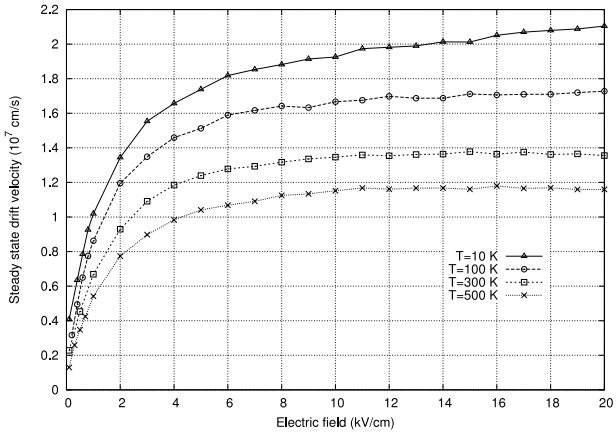

FIG. 3. Steady state drift velocities as a function applied field at various temperatures for dirty graphene ($n_i = 1.5 \times 10^{11}$ cm^{-2}, $D_{ac} = 20$ eV and $D_o = 1 \times 10^9$ eV/cm).

The behaviour of steady state velocity of monolayer dirty graphene for various temperatures is shown in Fig. 3. The parameters are the same as in Fig. 2 for the case of dirty graphene. The velocity increases steadily and reaches a saturation value with the applied field without any NDR effect. The velocity decreases as the temperature increases because the acoustic phonon scattering increases linearly with temperature. The temperature dependence of optic phonon scattering for graphene is very weak and the interface roughness scattering is independent of temperature. Therefore the temperature dependence of steady state velocity mainly comes from acoustic phonons.

The mobility of electrons for the graphene sheet is considered next for the case of intrinsic graphene as a function of temperature at a low electron concentration n. The acoustic deformation constant is $D_{ac} = 3.7$ eV. The behaviour of mobility as a function of temperature for $n = 1 \times 10^{12}$ cm^{-2} (empty diamonds) is shown in Fig. 4. These mobility values are obtained from the conductivity calculations by using equation (13). Our results are compared with the work of others in the literature. The values shown with empty triangles are from Ref. 11 for the case of low electron concentration $n = 1 \times 10^{12}$ cm^{-2} where they have taken into account acoustic, optic and surface polar phonon (SPP) scatterings. The agreement is good even if we neglect the SPP scattering. For low electron concentrations the fermi energy $E_F = \hbar\sqrt{\pi n}$ is low compared to optic phonon energies and therefore the scatterings due to optic phonons do not contribute to conductivity in any considerable manner (see eqn. (9)). Therefore one can assume that the mobility limiting mechanism at low electron concentrations is acoustic phonons. Although acoustic and optic phonon scatterings

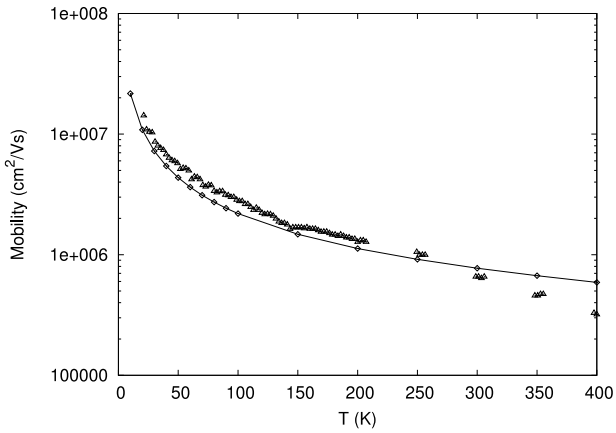

FIG. 4. The mobility values for intrinsic graphene (empty) diamonds. The empty triangles are from Ref. 11. See the text for details.

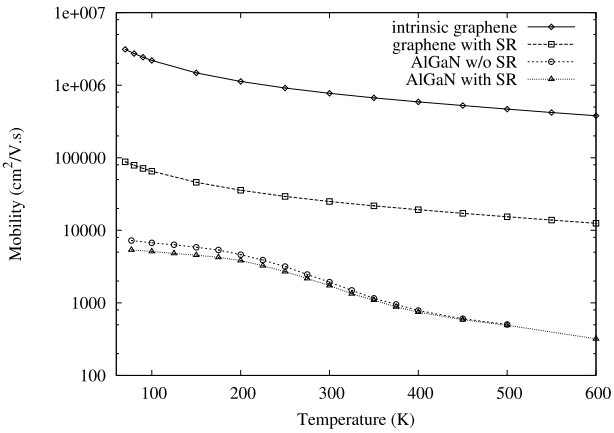

FIG. 5. Comparison of mobility values for monolayer graphene in the absence (empty diamonds) and presence (empty squares) of interface roughness scattering in addition to acoustic and optic phonon scatterings. These are compared with the mobility of two dimensional electrons at an AlGaN/GaN heterojunction from Ref. 30.

are independent of electron concentration, the surface polar phonon scattering is expected to depend on n.[11,18]

Finally we consider the mobility of electrons in the graphene sheet in the presence of interface roughness scatterings in addition to phonon scatterings. The mobility values are shown in Fig. 5 (empty squares) where interface roughness parameters are the same as in Fig. 2. The results for intrinsic graphene are also shown for reference purposes (empty diamonds). These results are compared with the mobility of two dimensional electrons at an AlGaN/GaN heterojunction from Ref. 30 (empty triangles and circles). As can be seen interface roughness can be very effective in limiting the mobility of electrons in graphene and can create an order of magnitude difference in mobility. GaN based devices are attracting a great deal of interest presently and as can be seen in Fig. 5 their mobilities are lower by an order of magnitude than the case where interface roughness is present and and by two orders of magnitude than intrinsic graphene sample.

IV. CONCLUSIONS

The transport properties of monolayer graphene is studied by an ensemble Monte Carlo technique. Both an intrinsic and dirty graphene samples are considered. For the intrinsic case acoustic and optic phonon scattering mechanisms, and in addition to these both ionized impurity and interface roughness scatterings are considered for the dirty graphene case. Undershoot effect is observed for intrinsic graphene for certain values of applied field and it disappears as the applied field increases. Velocity overshoot takes place at all field values and the peak velocity attained at a given applied field increases with the field. While negative diferential resistance is observed for low values of acoustic deformation potential constant (D_{ac} = 3.7 eV) for intrinsic graphene, it disappeares for high values of D_{ac} (D_{ac} = 20 eV) because acoustic phonon scattering becomes the dominant scattering mechanism compared to optic phonons.

The mobility of electrons are calculated for both intrinsic and graphene with interface roughness as a function of temperature from conductivity calculations. These mobility values are compared with those of two dimensional electrons at an AlGaN/GaN hetero junction. Interface roughness scattering is independent of temperature and therefore persists at all temperatures and is effective in limiting the mobility of electrons in monolayer graphene.

ACKNOWLEDGEMENTS

The work presented in this paper is supported by Cukurova University Research Fund No:FEF2012D18.

[1] K S Novoselov, A K Geim, S V Morozov, D Jiang, Y Zhang, S V Dubonos, I V Grigorieva, and A A Firsov, Science **306**, 666 (2004).
[2] A H Castro Neto, F Guinea, N M R Peres, K S Novoselov, and A K Geim, Rev. Mod. Phys. **81**, 109 (2009).
[3] C W J Beenakker, Rev. Mod. Phys. **80**, 1337 (2008).
[4] S Das Sarma, S Adam, E H Hwang, and E Rossi, Rev. Mod. Phys. **83**, 407 (2011).
[5] J S Bunch, A M van der Zande, S S Verbridge, I W Frank, D M Tanenbaum, J M Parpia, H G Craighead, and P L McEuen, Science **315**, 490 (2007).
[6] K I Bolotin, K J Sikes, Z Jiang, G Fudenberg, J Hone, P Kim, and H L Stormer, Solid State Commun. **146**, 351-355 (2008).
[7] W Zhu, V Perebeinos, M Freitag, and P Avouris, Phys. Rev. B **80**, 235402 (2009).
[8] J-H Chen, C Jang, S Adam, M S Fuhrer, E D Williams, and M Ishigami, Nature Physics **4**, 377-381 (2008).
[9] J-H Chen, C Jang, S Xiao, M Ishigami, and M S Fuhrer, Nat. Nanotechnol. **3**, 206-209 (2008).
[10] Y-W Tan, Y Zhang, H L Stormer, and P Kim, Eur. Phys. J. Special Topics **148**, 15-18 (2007).
[11] V Perebeinos and P Avouris, Phys. Rev. B **81**, 195442 (2010).
[12] K I Bolotin, K J Sikes, J Hone, H L Stormer, and P Kim, Phys. Rev. Lett. **101**, 096802(4) (2008).
[13] X Du, I Skachko, and E Y Andrei, Nature Nano **3**, 491-495 (2008).
[14] X Du, I Skachko, and E Y Andrei, Int. J. Mod. Phys. B **22**, 4579-4588 (2009).
[15] R S Shishir and D K Ferry, J. Phys.: Condens. Matter **21**, 344201 (2009).
[16] T Fang, A Konar, H Xing, and D Jena, Phys. Rev. B **84**, 125450 (2011).
[17] J Chauhan and J Guo, Appl. Phys. Lett. **95**, 023120 (2009).
[18] X Li, E A Barry, J M Zavada, M Buongiorno Nardelli, and K W Kim, Appl. Phys. Lett **97**, 232105 (2010).
[19] E H Hwang and S Das Sarma, Phys. Rev. B **77**, 115449(6) (2008).
[20] E H Hwang, S Adam, and S Das Sarma, Phys. Rev. Lett. **98**, 186806(4) (2007).
[21] S Adam, E H Hwang, V M Galitski, and S Das Sarma, Proc. Natl. Acad. Sci. **104**, 18392(6) (2007).
[22] T Stauber, N M R Peres, and F Guinea, Phys. Rev. B **76**, 205423(10).
[23] S Adam, E H Hwang, and S Das Sarma, Physica E **40**, 1022-1025 (2008).
[24] S Adam, E H Hwang, E Rossi, and S Das Sarma, Solid State Commun. **149**, 1072-1079 (2009).
[25] S Fratini and F Guinea, Phys. Rev. B **77**, 195415(6) (2008).
[26] T Ando, Journal of the Physical Society of Japan **75**, 074716 (2006).
[27] F Gamiz and J B Roldan, J. Appl. Phys. **94**, 392 (2003).
[28] R S Shishir, F Chen, J Xia, N J Tao, and D K Ferry, J. Comput. Electron. **8**, 43-50 (2009).
[29] W A Hadi, M S Shur, and S K OLeary, J. Appl. Phys. **112**, 033720 (2012).
[30] M Demir, Z Yarar, and M Ozdemir, Solid State Commun. B **158**, 29-33 (2013).